Quasi-equilibrium phase separation in supercritical fluids

Seungtaek Lee
Pohang University of Science and Technology (POSTECH) https://orcid.org/0000-0002-3292-4967
Juho Lee
Pohang University of Science and Technology (POSTECH)
Yeonguk Kim
Pohang University of Science and Technology (POSTECH)
Seok Jeong
Department of Physics, Pohang University of Science and Technology
Dong Eon Kim (kimd@postech.ac.kr)
Max Planck POSTECH/KOREA Res. Init. / POSTECH
Gunsu Yun (gunsu@postech.ac.kr)
Pohang University of Science and Technology (POSTECH) https://orcid.org/0000-0002-1880-5865

Article

Keywords: phase separation phenomenon, supercritical fluids, LL-GL phase separation, clustering

Posted Date: July 17th, 2020

DOI: https://doi.org/10.21203/rs.3.rs-38529/v1

Version of Record: A version of this preprint was published at Nature Communications on July 30th, 2021. See the published version at https://doi.org/10.1038/s41467-021-24895-y.

Quasi-equilibrium phase separation in supercritical fluids

Seungtaek Lee [1], Juho Lee [1], Yeonguk Kim [1], Seokyong Jeong [1], Dong Eon Kim [1, 2 *], Gunsu Yun [1, 2, 3 †]

[1] Department of Physics, Pohang University of Science and Technology, Pohang, 37673, Republic of Korea

[2] Max Planck Center for Attosecond Science, Max Planck POSTECH/KOREA Research Initiative, Pohang, 37673, Republic of Korea

[3] Division of Advanced Nuclear Engineering, Pohang University of Science and Technology, Pohang, 37673, Republic of Korea

[*] kimd@postech.ac.kr

[†] gunsu@postech.ac.kr

Correspondence and requests for materials should be addressed to Dong Eon Kim or Gunsu Yun.

Abstract

This study describes the discovery of a phase separation phenomenon in supercritical fluids (SCFs). An SCF is technically a single-phase fluid with two sub-domains separated by the Widom line. A pseudo phase transition occurs between liquid-like (LL) and gas-like (GL) states, similar to the gas-liquid phase transition across the coexistence line in subcritical fluids. By extending the analogy, we demonstrate that LL-GL phase separation is possible by generating submicron size LL argon droplets in a GL argon SCF. The GL fluid is in a quasi-equilibrium clustered state well above the critical temperature, with a significant increase in cluster formation rate traversing the critical pressure. The prolonged phase separation over an hour is consistent with a model of mass transport mediated by clusters. It provides the insight that clustering is an essential factor in transport and non-equilibrium thermodynamic processes in SCFs.

Introduction

Supercritical fluids (SCFs), first discovered in 1822 by Charles Cagniard de la Tour [1], have attracted continuous scientific and industrial interests owing to their unique properties such as higher density compared to the gas phase, lower viscosity compared to the liquid phase, and intrinsically high level of density fluctuations [2, 3]. The lower viscosity, higher diffusivity, and superior solubility compared to liquid counterparts mean that SCFs can enable enhanced chemical reaction rates [4]. Some of the applications of SCFs that have been extensively investigated include the selective extraction of molecules from natural materials [5] and the synthesis of polymer nanocomposite foams [6, 7]. They can also be used as refrigerants in a heat pump system [8], and as reaction media for chemical processes [9].

It is a common belief that there is no phase separation in SCFs, unlike the subcritical fluids that have distinct liquid and vapor phases. SCFs far from the critical point are homogeneous and structureless, due to which they do not have any surface tension or phase transition. However, over the last two decades, it has been observed that SCFs have two distinct domains: a liquid-like (LL) state and a gas-like (GL) state [10, 11]. The two domains are separated by the Widom line, which corresponds to the extrema of a thermodynamic response function (e.g., specific heat capacity and compressibility). The line is a continuation of the gas-liquid phase boundary extending from the critical point. The change between LL and GL states is called a 'pseudo' phase transition, as no singularity occurs at the Widom line. The LL and GL properties of SCFs have been confirmed through experiments as well as molecular dynamics simulations over a wide range of temperature and pressure conditions across the Widom line [12–15].

It is worth noting that the LL and GL states of an SCF considered in those studies are equilibrium states. This notion brings about an intriguing question whether a non-equilibrium or quasi-equilibrium LL phase can coexist in a GL SCF medium, that is, whether a quasi-equilibrium phase separation is possible in SCFs. This question is relevant to many natural and industrial processes that involve dynamic flows of SCFs, such as meteorological processes in the atmosphere of Venus and SCF extraction [16].

The quasi phase separation in SCFs may be expected by extending the concept of coexistence in subcritical fluids. In the subcritical phase, a phase-mixed state of liquid and gas is stable along a binodal curve called the coexistence line in the density-temperature (or concentration-temperature) diagram, and metastable in an extended region close to the coexistence line [17]. The liquid and the gas phases separate permanently below the metastable region at a distance from the coexistence line. A quasi-stable pseudo phase separation, similar to the stable phase separation in the subcritical region, may occur in SCF.

In this study, we experimentally demonstrate, for the first time, a distinct phase separation of GL states and LL states in SCF, produced through a compression-expansion process using argon as an archetypal inert species. It is clearly observed that the characteristics of SCF dramatically change across the critical pressure but well above the critical temperature in terms of a sudden formation of droplets, a sudden drop of their lifetime, and a sudden increase of opacity. These droplets coexist with the background GL medium for a long time. We find that the clustering in the medium plays a significant role in the surface transport at the interface between the LL droplet and GL fluid. It is well known that the degree of intrinsic clustering in SCF, which occurs via a density fluctuation, reaches the maximum at the critical point [3] and diminishes above the critical point as manifested by the decrease of the intrinsic density fluctuations. Our study shows that this conventional knowledge is incomplete and confirms that a considerable clustering due to external perturbations can occur in the SCF region across the critical pressure but well above the critical temperature. Based on a quasi-equilibrium model of surface transport, we illustrate how the evaporation of an LL droplet in a GL SCF, mediated by the clusters, differs from subcritical evaporation. The concept of this pseudo-evaporation of LL droplets in GL fluid was not recognized previously because most of the studies focused on the observations of equilibrium thermodynamic properties and pseudo phase transition. This observation could be a manifestation of 'pseudo'-evaporation of LL droplets in GL fluid.

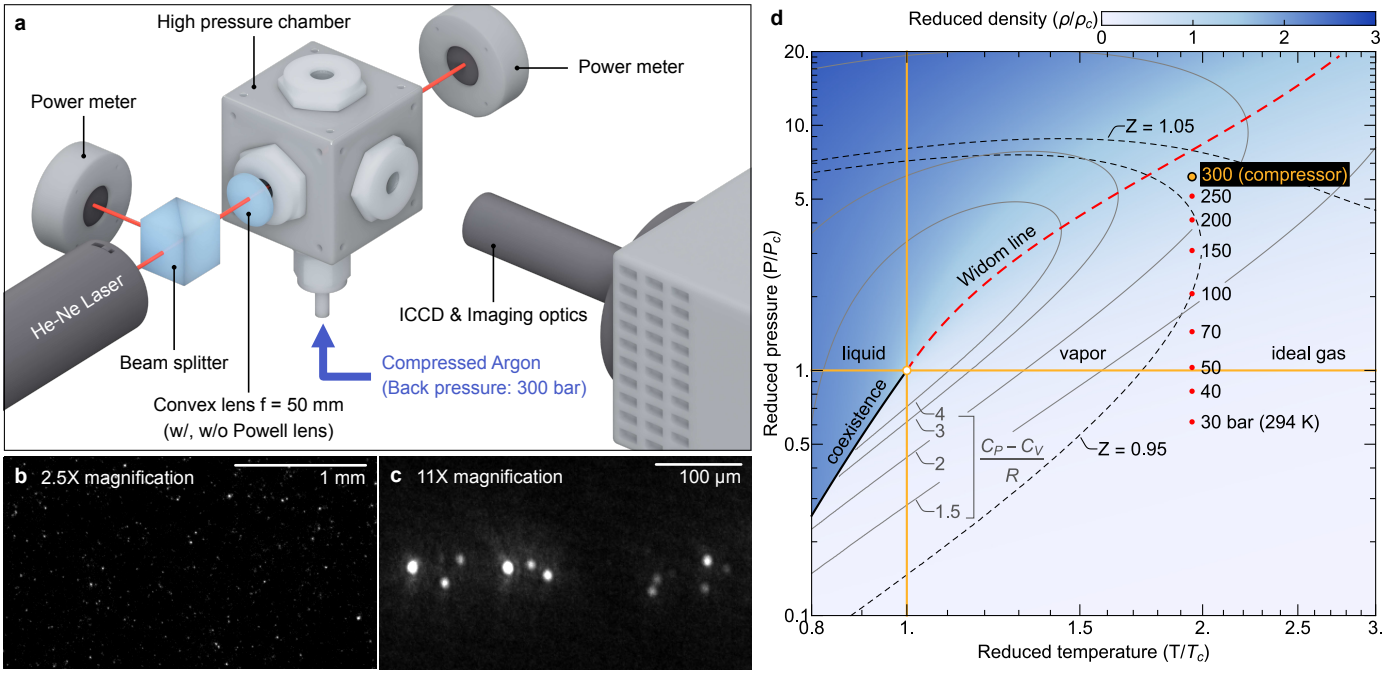

Fig.1 Experimental apparatus and conditions. **a**. Schematic of the high-pressure chamber system. The incident He-Ne laser (633 nm, 5 mW) has a beam waist radius of about 50 μm at the focus. The incident laser is additively reshaped with a laser line generator (called the Powell lens) in case that the magnification of imaging optics is low. Imaging optics and intensified CCD (ICCD) capture the Rayleigh–Mie scattering signals from individual droplets. **b-c.** Images of droplets with 2.5X and 11X magnifications at 100 bar. **d.** Extended phase diagram of argon. The red points indicate the experimental conditions. The working pressure of the compressor is 300 bar. The compressibility factor $Z = P/\rho RT$ shows the deviation from an ideal gas. The thermophysical properties of argon are obtained from the NIST Chemistry WebBook [18].

Results

Experimental apparatus and conditions

A reciprocating compressor delivers argon fluid into the high-pressure chamber through a check valve (opening pressure: 300 bar). With each cycle, the compressor supplies ~ 7 cm^3 of argon fluid (under the standard condition). A series of experiments has been carried out along the line of red points shown in Fig.1**d** (the extended phase diagram of supercritical argon) [19]. The argon fluids in these conditions can be approximated as an ideal gas in equilibrium. Because the temperature is about two times the critical temperature, spontaneous critical phenomena such as density fluctuations do not occur; however, the fluid undergoes a sudden expansion and cools to form liquid-like droplets and clusters in the process of filling the chamber with argon.

The imaging optics with the ICCD camera captures images and videos of droplets with two different magnifications (2.5X and 11X). The droplets are individually identified owing to their higher Rayleigh–Mie scattering intensity compared to the scattering intensity of the argon fluid and clusters in the background. The number density and the mean size of droplets are obtained from the lower- and higher-magnification data, respectively. Note that the size of individual droplets cannot be measured by direct imaging because of the diffraction limit of the visible light (light source: 633 nm He–Ne laser). Hence, Brownian motion analysis is adopted to determine the mean size of the droplets.

Formation of droplets and clusters

Fig.2 shows how the SCF properties change with the increase of pressure in terms of droplet density, the average lifetime of droplets, and medium opacity. We note the dramatic changes of these properties across the critical pressure. Fig.2**a** shows the sudden increase of the droplet density across the critical pressure, above which it is saturated. The argon gas is cumulatively compressed into the chamber through the check

valve while creating LL droplets and clusters [20–22]. As the operating pressure of the check valve (300 bar) is fixed, the rate at which the droplets are generated decreases as the chamber pressure increases, and eventually, the droplet formation stops. The droplets produced during the compression also undergo pseudo-evaporation within the fluid. Thus, the number density of droplets does not keep increasing throughout the compression, as shown in Fig.2**a**. Instead, the generation and pseudo-evaporation of the droplets occur simultaneously and compete.

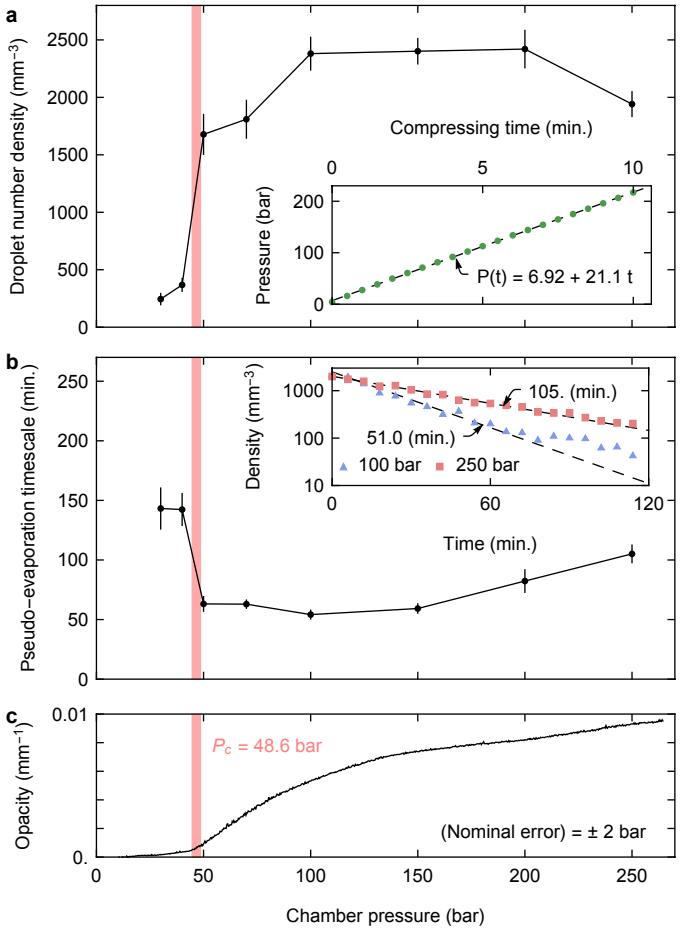

Fig.2 Presence of droplets and clusters. **a**. The number density of droplets generated by the continual compression of argon fluid in the high-pressure chamber. The droplet number density decreases as the pressure exceeds 150 bar because the droplet formation becomes less efficient at a higher chamber pressure (i.e., a smaller pressure difference between the chamber and check valve) and the droplets pseudo-evaporate. The number density of droplets decreases due to pseudo-evaporation in the medium. **b**. The pseudo-evaporation timescale at different pressures. **c**. The major contribution to medium opacity comes from clusters.

The lifetime of droplets or the pseudo-evaporation timescale (measured by the time when the droplet number density becomes 1/10th of the maximum) at different chamber pressures is shown in Fig.2**b**. For each pressure condition, the droplet number density is tracked for two hours after the compression. As the chamber pressure increases above the critical pressure, the pseudo-evaporation timescale suddenly decreases and then increases. In the following section, we explain both the discontinuous change near the critical pressure and the monotonic elevation at higher pressures based on the pseudo-evaporation model and the resulting cluster effect.

As shown in Fig.2**c**, the opacity inside the chamber rapidly increases, which we attribute to the generation of a large number of clusters. Note that these clusters are not spontaneously produced by critical phenomena but by a compression-expansion process.

Unlike droplets, the clusters are too small to be individually identified. They increase the medium opacity through the Rayleigh scattering and absorption. To clarify that the major contribution to the opacity is from these clusters, rather than the droplets, we estimate the opacity due to the scattering by droplets:

$$\chi_{\mathrm{d}} \sim n_{\mathrm{d}}\sigma_{\mathrm{d}} \sim n_{\mathrm{d}}\pi r_{\mathrm{d}}^2 \qquad (1)$$

where the subscript d stands for the droplets and n, r, and σ are the number density, mean radius of droplets, and the total cross-section of the Rayleigh scattering and absorption, respectively [23, 24]. The upper limit of the opacity caused by the droplets is about $0.002\,\mathrm{mm}^{-1}$ (using $n_{\mathrm{d}} \sim 2500\,\mathrm{mm}^3$ around 150 bar and $r_{\mathrm{d}} \sim 0.5 \times 10^{-3}$ mm, see Fig.3), which is quite small, implying that the major contribution to opacity comes from the clusters and not from droplets. The clusters are the leading cause of the fogginess and opacity of the medium.

It turns out that a large number of clusters in the argon fluid also has a significant effect on the mass transport at the droplet surface, as we discuss below. The clustering in the GL medium affects the pseudo-evaporation timescale of the phase-separated LL droplets.

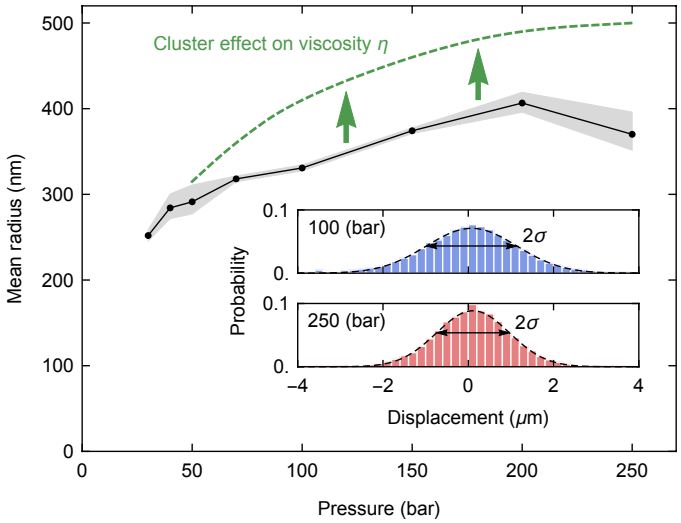

Fig.3 Mean size of droplets at different pressures. Brownian motion analysis is adopted to measure the mean size at each pressure. The medium viscosity tends to decrease with the appearance of the clusters. The green dashed line depicts the change in estimated droplet sizes, taking into account the cluster effect on the viscosity in a situation where the cluster density is high as in our experiments.

Droplet size

A large number of submicron-size LL droplets floating in the argon SCFs are visually identified. Notably, the pseudo phase separation (i.e., LL droplets in the GL medium) persists for a long time, which enabled us to apply the direct imaging and the Brownian motion analysis to find the size of droplets.

The mean size of droplets is measured by considering them as Brownian particles floating in the argon fluid. The small displacements of droplets from their jiggling motion are tracked by high-resolution imaging optics (11X magnification) and ICCD (50 frames per second). The videos are captured 3 minutes after the compression allowing any turbulence in the medium to be stabilized at each pressure condition.

The mean squared displacement σ^2 of Brownian particles is expressed by the following equation [25]:

$$\sigma^2 = 2Dt \qquad (2)$$

where D is the diffusion coefficient of the surrounding medium and t is the elapsed time (in our experiment, $t = 0.02$ s). The diffusion coefficient is related to the mean radius r of the Brownian particles through the Stokes–Einstein equation [25]:

$$D = \frac{k_B T}{6\pi\eta r} \qquad (3)$$

where k_B, T, and η are the Boltzmann constant, the temperature, and the dynamic viscosity of the surrounding medium, respectively. The dynamic viscosity of argon at each pressure value can be obtained from the NIST Chemistry WebBook [18]. The mean radius of the droplets, based on the dynamic viscosity,

varies from about 250 to 400 nm depending on the final chamber pressure, as shown in Fig.3. However, if the medium contains a large number of clusters, using a homogeneous medium viscosity may introduce errors in size estimation. When some portions of the medium are clustered, the viscosity tends to be lower than that of the homogeneous medium, and as a result, it leads to an underestimation of the droplet size. We will discuss this further in the discussion section.

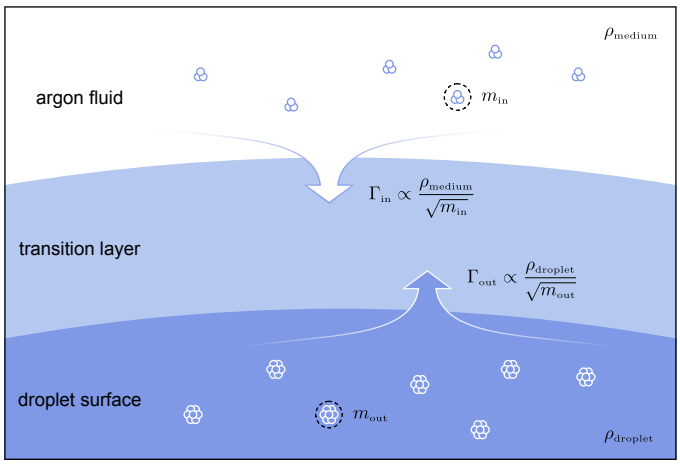

Fig.4 Graphical illustration of the mass transport at a droplet surface. The emergence of clusters reduces the mass influx, and consequently, the pseudo-evaporation time of a droplet decreases.

Droplet lifetime: cluster effect on pseudo-evaporation

The trend of the estimated droplet radii around the critical pressure (Fig.3) appears to contradict the trend of the droplet lifetime (the pseudo-evaporation timescale) (Fig.2**b**). The two trends may imply that the smaller droplets below the critical pressure would take longer to pseudo-evaporate than the larger droplets above the critical pressure. This apparent contradiction is resolved by considering the effect of clusters on the mass transport at the droplet surface.

It is impractical to consider all the interactions among the atoms in a submicron-size droplet in the dense background fluid to evaluate the pseudo-evaporation timescale. Instead, a submicron-size LL droplet is large enough to regard the pseudo-evaporation as a surface process. Thus, we adopt an evaporation model similar to that of subcritical fluids to explain our experimental results [26, 27].

The prolonged survival over an hour implies that the droplet and the surrounding fluid are in a quasi-thermal equilibrium and that the mass influx Γ_{in} would balance the mass outflux Γ_{out} in the transition layer around the droplet surface (Fig.4), indicating that the net mass flux Γ_{net} is negligible:

$$\begin{aligned} \Gamma_{\mathrm{net}} &= \Gamma_{\mathrm{out}} - \Gamma_{\mathrm{in}} \\ &= v_{\mathrm{out}}\rho_{\mathrm{out}} - v_{\mathrm{in}}\rho_{\mathrm{in}} \approx 0 \end{aligned} \qquad (4)$$

where $v_{\mathrm{in(out)}}$ and $\rho_{\mathrm{in(out)}}$ are the surface-normal mean velocities and mass densities, respectively. The outflux is defined as the flux leaving the inner boundary of the transition layer, i.e., the surface of the droplet. The surface-normal mean velocity is then

$$v_{\mathrm{in\ (out)}} = \sqrt{\frac{8k_B T}{\pi m_{\mathrm{in\ (out)}}}} \propto \frac{1}{\sqrt{m_{\mathrm{in\ (out)}}}} \qquad (5)$$

where $m_{\mathrm{in\ (out)}}$ denotes the mass of the mass carrier. The droplet is assumed to have a Widom line crossing density ($\rho_{\mathrm{out}} = \rho_{\mathrm{droplet}} = \rho_{\mathrm{Widom}}$) at a given temperature, based on the analogy that the LL droplet is in a saturated condition in the subcritical state. Thus, the net mass flux can be written as

$$\Gamma_{\mathrm{net}} \propto \frac{\rho_{\mathrm{droplet}}}{\sqrt{m_{\mathrm{out}}}} - \frac{\rho_{\mathrm{medium}}}{\sqrt{m_{\mathrm{in}}}} \qquad (6)$$

where the mass density of influx $\rho_{in} = \rho_{medium}$. When the net flux stays negligible, the pseudo-evaporation timescale would be extended.

During compression, the number of clusters in the medium rapidly increases when crossing the critical pressure, and m_{in} becomes clustered. Thereby, the influx significantly reduced, and as a result, the pseudo-evaporation timescale shortened. On the other hand, under subcritical pressures, the number of clusters is fewer; therefore, the influx is significant, resulting in a much longer pseudo-evaporation timescale. If the pressure continues to increase and exceeds the critical pressure, the number of clusters also increases. However, as ρ_{medium} gradually approaches $\rho_{droplet}$, the overall flux is rebalanced, resulting in a prolonged pseudo-evaporation timescale.

Discussion and conclusion

The size estimation by the Brownian motion analysis obtained through Eq.(3) depends on the accuracy of the medium viscosity. In our study, we used the viscosity value corresponding to a homogeneous argon fluid at the given pressure and temperature, taken from the NIST Chemistry WebBook [18]. However, as the pressure increases, more clusters are generated in the medium, and it is necessary to understand how this will affect the viscosity of the fluid. Instead of a comprehensive analysis of the viscosity, a simplified analysis is sufficient to show that the viscosity of the medium containing clusters would be lower than that of the homogeneous medium.

According to the kinetic model, the viscosity η of a medium consisting of spherical particles of radius r and mass m is

$$\eta \propto \frac{\sqrt{mT}}{\pi r^2} \qquad (7)$$

where T is the temperature of the medium [28]. When considering the interaction between particles, the proportionality constant may have a temperature dependence, but the fundamental relationship does not change significantly. Assuming that an individual cluster consists of N argon atoms on an average and the temperature is fixed,

$$\eta \propto N^{-1/6} \qquad (8)$$

as $m \propto N$ and $r \propto N^{1/3}$. Thus, the viscosity of the medium decreases if atoms aggregate to form clusters; consequently, the droplet size is underestimated for a higher cluster density. This cluster effect on the estimation of droplet size is illustrated by a green dashed curve in Fig.3.

In summary, we demonstrate that pseudo phase separation, i.e., LL droplets in a GL medium, is possible in non-equilibrium SCFs. The analysis of mass transport shows that the clustering can reduce the pseudo phase separation of an SCF, indicating that the clustering effect plays an essential role in the understanding of phase separation and other thermodynamic processes in supercritical states.

The existence of quasi-steady clustering and pseudo-phase separation will have practical implications in various fields of science and engineering involving SCFs such as planetary meteorology, power plant cooling systems, pharmaceutical processes, and high-power switching. For instance, the clusters and droplets may affect the mass transport processes in the dense atmospheres of Venus and Jupiter. The same effect may have to be considered in the recent development of the SCF CO_2 cleaning technique in semiconductor fabrication.

We expect our findings to serve as an important milestone in exploring pseudo-phase-separation phenomena beyond the fact that SCFs are separated into two distinct regions with LL and GL properties. The physics underlying the formation of the LL droplets, i.e., the process of the pseudo phase separation, will be an immediate topic of interest, and theoretical studies and computer simulations will be required to better understand the surface transport processes in SCFs.

Methods

High-pressure chamber system

The reciprocating compressor has a cycling frequency of about 4.1 Hz and a throughput of about 6.8 cm^3/cycle (under standard conditions). A pair of bendable stainless-steel hoses (Swagelok SS-FX4TA4TA4) is installed to add flexibility to the system. Quick-connect adapters (SS-QF4-S, SS-QF4-B) are placed at the junctions, which modularize the system and thereby make it possible to carry the chamber after compression. The cubic-shaped stainless-steel chamber (side length: 65 mm) is computer numerical control (CNC) machined to make six threading ports (1 1/16”-12-UN) with O-ring grooves (SAE J1926-1). One of the ports is used as the gas entrance, and sight windows are installed on the other ports. The sight windows, made of sapphire glass (thickness: 7.2 mm) and bonded in the stainless-steel housing, has a clear aperture 11.2 mm in diameter (Rayotek 101117C). Two different pressure sensors, one with a digital display (Keller LEO2) and the other with an analog voltage output (Tival Sensors TST-20) are installed to monitor the pressure for safety.

Laser scattering

A vertically polarized continuous He–Ne laser at 633 nm with 5 mW output power (Thorlabs HNL050LB) operates as the scattering source. Two lenses manipulate the beam profile of the incident laser: a plano-convex lens with a focal length of 50 mm (Thorlabs LA4148) and a laser line generator (or Powell lens) with a fan angle of 23° (Thorlabs FLG10FC-633). Right-angle scattered signals are captured by ICCD (Princeton Instruments PI-MAX4) with imaging optics. The imaging optics system enables 2.5X and 11X magnification through a single lens system with different optical lengths embedded into the lens tube to avoid ambient light (Thorlabs LA4148).

Particle tracking code

Custom-written Mathematica code (Wolfram Research 12.0 Student Edition) is used to analyze the images and videos. Two built-in functions (ComponentMeasurements and ImageFeatureTrack) are utilized to determine the number density of droplets from the images and the Brownian motion of droplets from the videos.

Acknowledgments

This study is supported by the National Research Foundation of Korea (NRF) funded by the Ministry of Science and ICT (No. 2019R1A2C3011474 and 2016K1A4A4A01922028) and Ministry of Education (No. 2019R1A6A3A13091407).

Author contributions

G.Y. proposed the original idea and conceived the project. S.L. and J.L. designed the high-pressure chamber system and performed the experiments. S.L. carried out the majority of the data processing and wrote the draft of the manuscript. S.L. and G.Y. analyzed the data of the Brownian motions and developed the pseudo-evaporation model. Y.K. and S.J. performed the molecular dynamics simulations to assist in the interpretation of the pseudo-evaporation model. G.Y. and D.K. supervised the project. All authors contributed significantly to the discussion of the results and the writing of the manuscript.

References

[1] Berche, B., Henkel, M. & Kenna, R. Critical phenomena: 150 years since Cagniard de la tour. *J. Phys. Stud.* **13**, 3001 (2009).

[2] Knez, Ž. et al. Industrial applications of supercritical fluids: A review. *Energy* **77**, 235–243 (2014).

[3] Stauss, S., Muneoka, H., Urabe, K. & Terashima, K. Review of electric discharge microplasmas generated in highly fluctuating fluids: Characteristics and application to nanomaterials synthesis. *Phys Plasmas* **22**, 057103 (2015).

[4] Medina, I. Determination of diffusion coefficients for supercritical fluids. *J. Chromatogr. A* **1250**, 124–140 (2012).

[5] Sovová, H. Steps of supercritical fluid extraction of natural products and their characteristic times. *J. Supercrit. Fluids* **66**, 73–79 (2012).

[6] Lee, L. J. et al. Polymer nanocomposite foams. *Compos. Sci. Technol.* **65**, 2344–2363 (2005).

[7] Matson, D. W., Fulton, J. L., Petersen, R. C. & Smith, R. D. Rapid expansion of supercritical fluid solutions: solute formation of powders, thin films, and fibers. *Ind. Eng. Chem. Res.* **26**, 2298–2306 (1987).

[8] Duffey, R. B. & Pioro, I. L. Experimental heat transfer of supercritical carbon dioxide flowing inside channels (survey). *Nucl. Eng. Des.* **235**, 913–924 (2005).

[9] Munshi, P. & Bhaduri, S. Supercritical CO_2 : a twenty-first century solvent for the chemical industry. *Curr. Sci.* **97**, 63–72 (2009).

[10] Simeoni, G. G. et al. The Widom line as the crossover between liquid-like and gas-like behaviour in supercritical fluids. *Nat. Phys.* **6**, 503–507 (2010).

[11] Gorelli, F., Santoro, M., Scopigno, T., Krisch, M. & Ruocco, G. Liquidlike behavior of supercritical fluids. *Phys. Rev. Lett.* **97**, 245702 (2006).

[12] Bolmatov, D., Brazhkin, V. V. & Trachenko, K. Thermodynamic behaviour of supercritical matter. *Nat. Commun.* **4**, 2331 (2013).

[13] Banuti, D. T. Crossing the Widom-line –supercritical pseudo-boiling. *J. Supercrit. Fluids* **98**, 12–16 (2015).

[14] Pipich, V. & Schwahn, D. Densification of supercritical carbon dioxide accompanied by droplet formation when passing the Widom line. *Phys. Rev. Lett.* **120**, 145701 (2018).

[15] Maxim, F. et al. Visualization of supercritical water pseudo-boiling at Widom line crossover. *Nat. Commun.* **10**, 4114 (2019).

[16] Taylor, L. *Supercritical Fluid Extraction (Techniques in analytical chemistry)* (Wiley, 1996).

[17] Dill, K. A. & Bromberg, S. *Molecular Driving Forces: Statistical Thermodynamics in Biology, Chemistry, Physics, and Nanoscience* (Garland Science, 2011), 2nd edn.

[18] Linstrom, P. J. & Mallard, W. G. *NIST Chemistry WebBook, NIST Standard Reference Database Number 69* (National Institute of Standards and Technology, Gaithersburg MD, 2020), https://webbook.nist.gov

[19] Banuti, D. T., Raju, M. & Ihme, M. Similarity law for Widom lines and coexistence lines. *Phys. Rev. E* **95**, 052120 (2017).

[20] Hagena, O. F. Nucleation and growth of clusters in expanding nozzle flows. *Surf. Sci.* **106**, 101–116 (1981).

[21] Chen, G., Kim, B., Ahn, B. & Kim, D. E. Pressure dependence of argon cluster size for different nozzle geometries. *J. Appl. Phys.* **106**, 053507 (2009).

[22] Tao, Y., Hagmeijer, R., van der Weide, E. T. A., Bastiaens, H. M. J. & Boller, K.-J. Revisiting argon cluster formation in a planar gas jet for high-intensity laser matter interaction. *J. Appl. Phys.* **119**, 164901 (2016).

[23] Fisák, J., Krticka, J., Munzar, D. & Kubát, J. Rayleigh scattering in the atmospheres of hot stars. *A&A* **590**, A95 (2016).

[24] van de Hulst, H. C. *Light Scattering by Small Particles* (Courier Corporation, 1981).

[25] Einstein, A. *Investigations on the Theory of Brownian Movements (translated by Cowper, A. D.)* (Dover, 1956).

[26] Ishiyama, T., Yano, T. & Fujikawa, S. Molecular dynamics study of kinetic boundary condition at an interface between argon vapor and its condensed phase. *Phys. Fluids* **16**, 2899–2906 (2004).

[27] Julin, J. et al. Mass accommodation of water: Bridging the gap between molecular dynamics simulations and kinetic condensation models. *J. Phys. Chem. A* **117**, 410420 (2013).

[28] Chapman, S., Cowling, T., Burnett, D. & Cercignani, C. *The Mathematical Theory of Nonuniform Gases: An Account of the Kinetic Theory of Viscosity, Thermal Conduction and Diffusion in Gases* (Cambridge University Press, 1990).

Figures

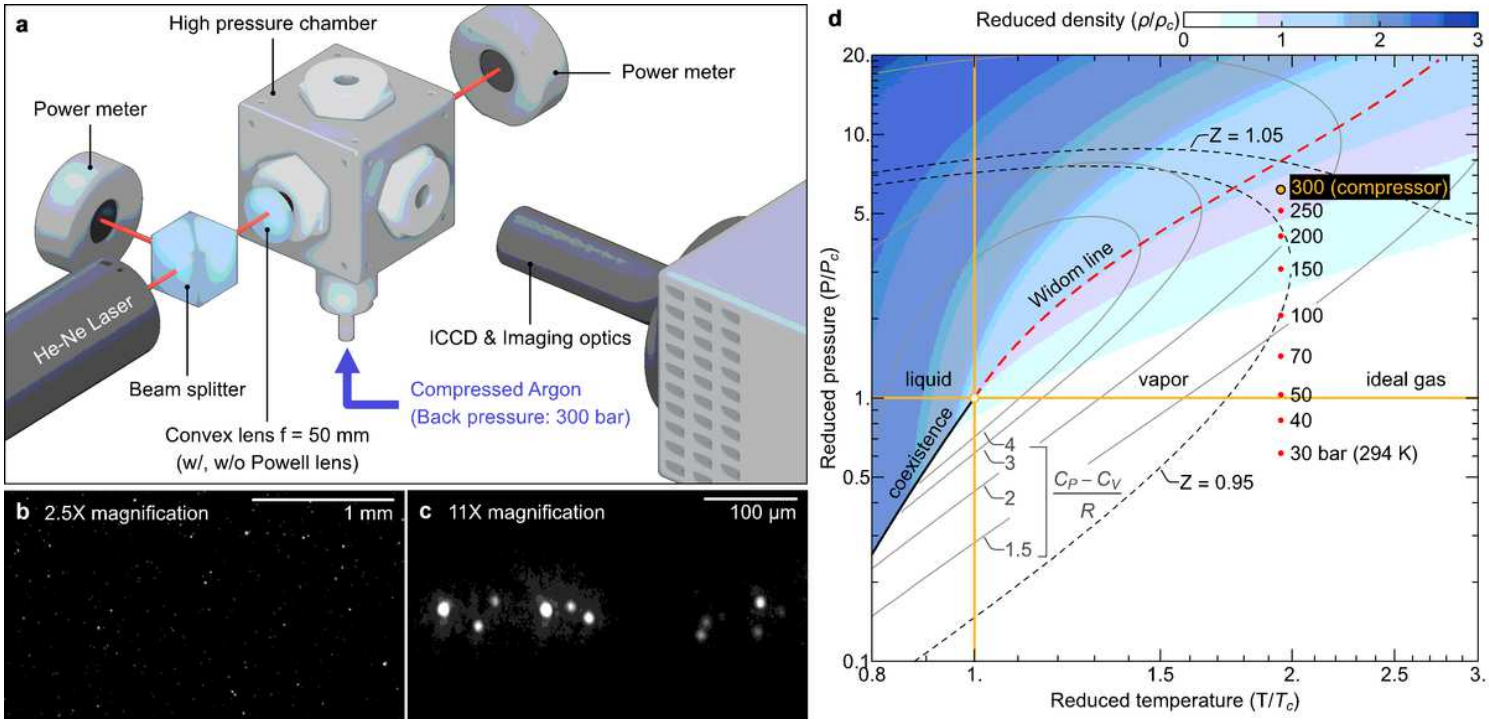

Figure 1

Experimental apparatus and conditions. a. Schematic of the high-pressure chamber system. The incident He-Ne laser (633 nm, 5 mW) has a beam waist radius of about 50 μm at the focus. The incident laser is additively reshaped with a laser line generator (called the Powell lens) in case that the magnification of imaging optics is low. Imaging optics and intensified CCD (ICCD) capture the Rayleigh–Mie scattering signals from individual droplets. b-c. Images of droplets with 2.5X and 11X magnifications at 100 bar. d. Extended phase diagram of argon. The red points indicate the experimental conditions. The working pressure of the compressor is 300 bar. The compressibility factor Z=P/ρRT shows the deviation from an ideal gas. The thermophysical properties of argon are obtained from the NIST Chemistry WebBook [18].

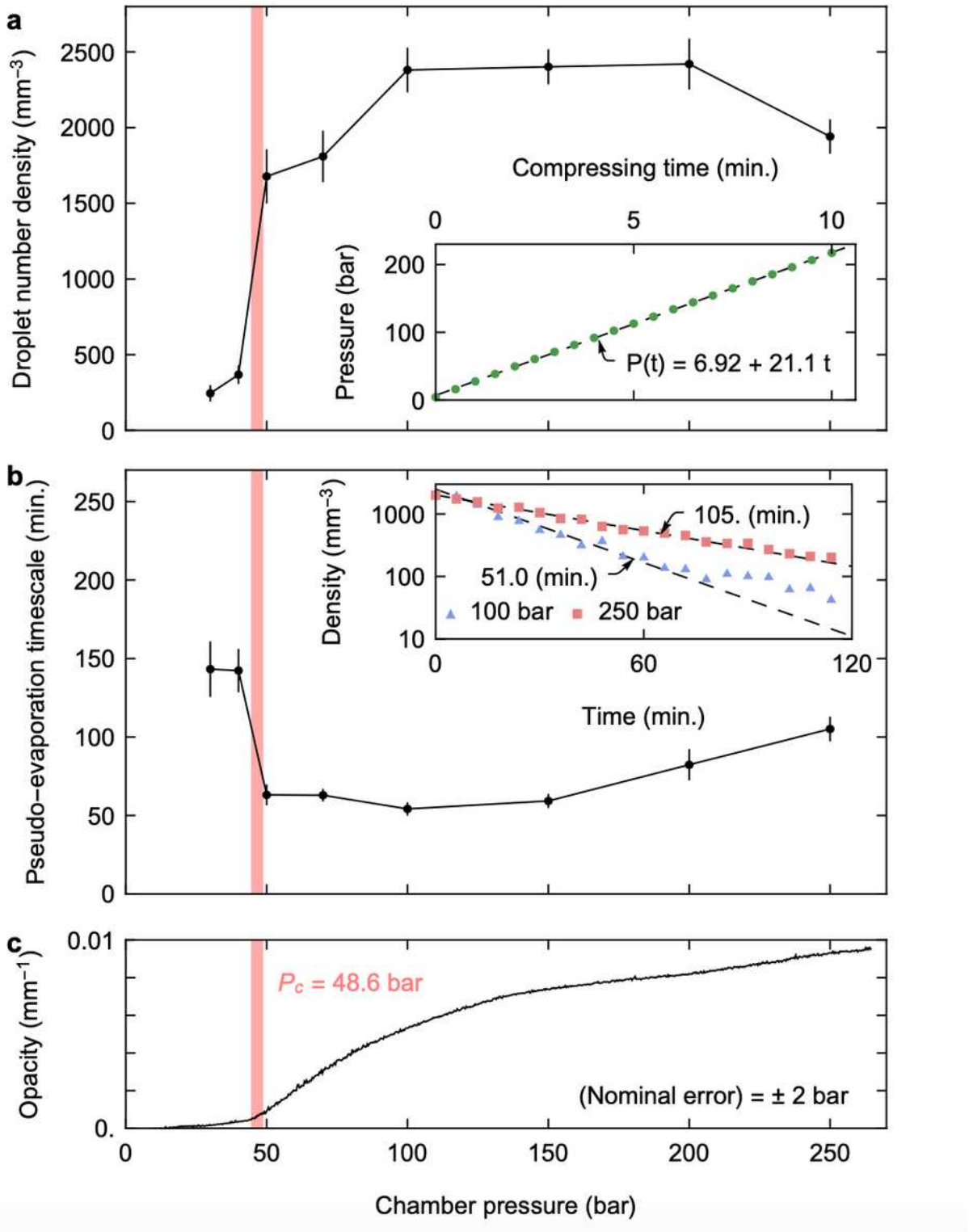

Figure 2

Presence of droplets and clusters. a. The number density of droplets generated by the continual compression of argon fluid in the high-pressure chamber. The droplet number density decreases as the pressure exceeds 150 bar because the droplet formation becomes less efficient at a higher chamber pressure (i.e., a smaller pressure difference between the chamber and check valve) and the droplets pseudo-evaporate. The number density of droplets decreases due to pseudo-evaporation in the medium.

b. The pseudo-evaporation timescale at different pressures. c. The major contribution to medium opacity comes from clusters.

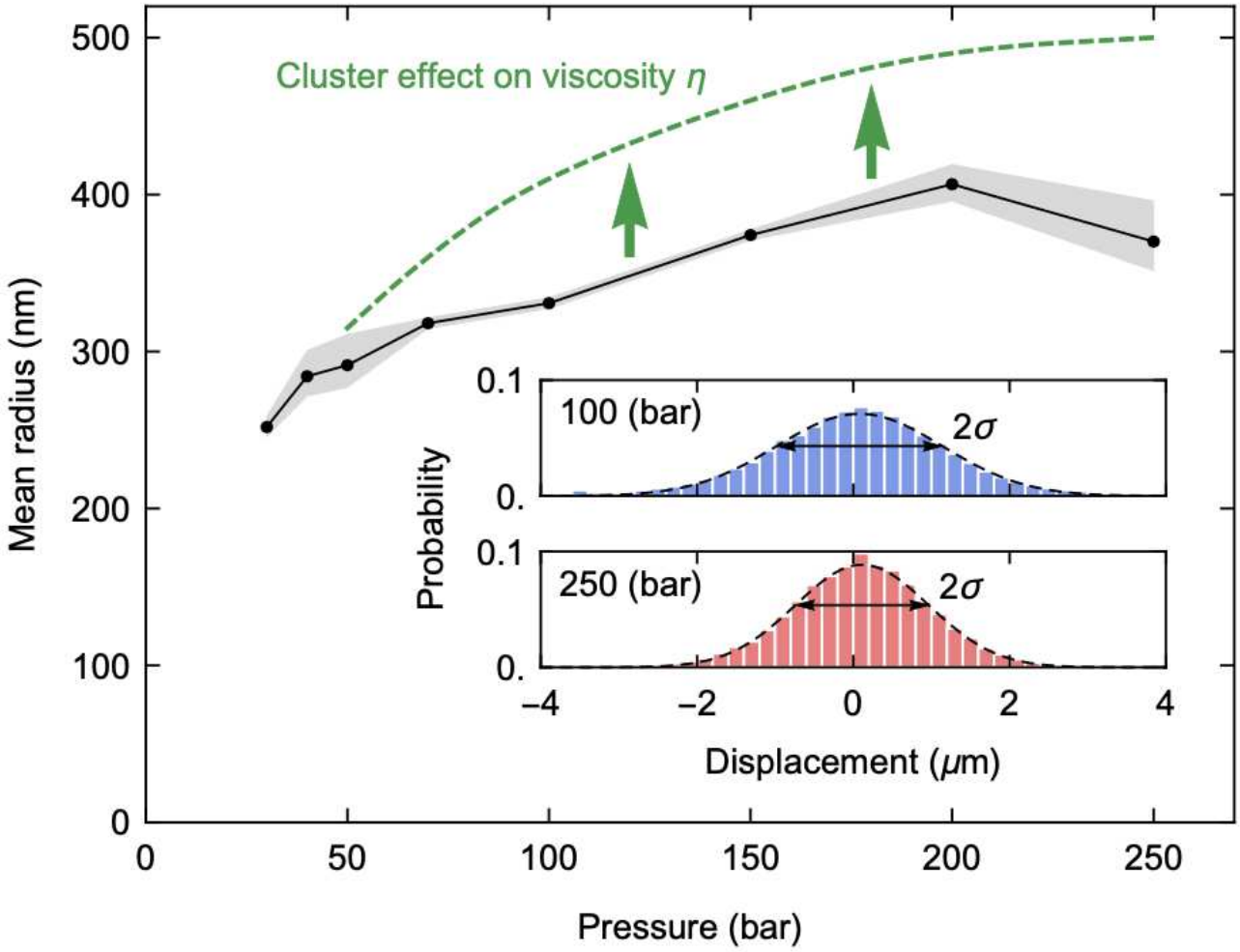

Figure 3

Mean size of droplets at different pressures. Brownian motion analysis is adopted to measure the mean size at each pressure. The medium viscosity tends to decrease with the appearance of the clusters. The green dashed line depicts the change in estimated droplet sizes, taking into account the cluster effect on the viscosity in a situation where the cluster density is high as in our experiments.

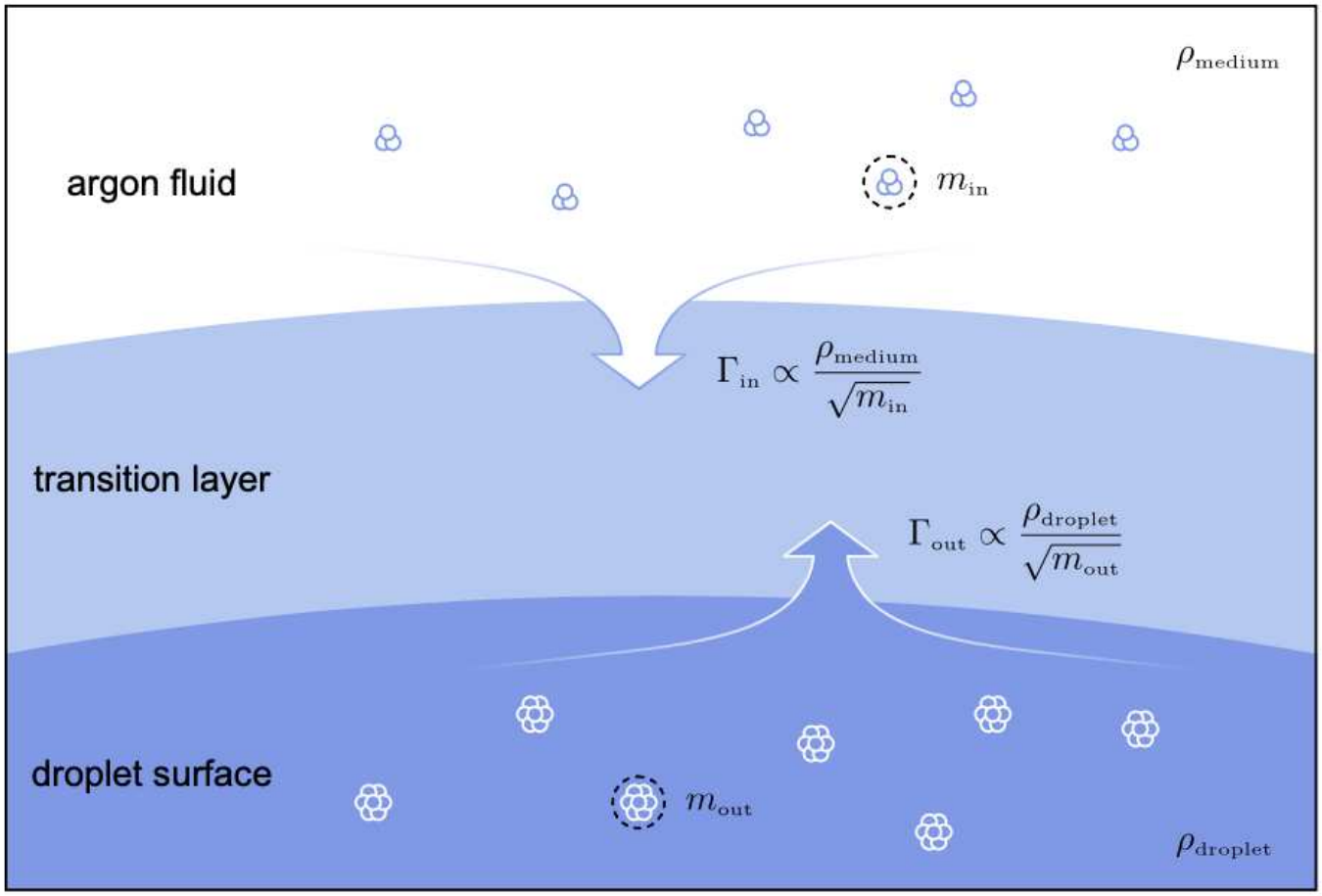

Figure 4

Graphical illustration of the mass transport at a droplet surface. The emergence of clusters reduces the mass influx, and consequently, the pseudo-evaporation time of a droplet decreases.